Global Low Harmonic Degree Models of the Seasonal Variability and Residual Ocean Tides from Topex/Poseidon altimeter data.

by

Per Knudsen[1]
Kort- og Matrikelstyrelsen
Rentemestervej 8
DK-2400 Copenhagen NV, Denmark

Abstract. The large scale seasonal variability is estimated jointly with the mean sea surface and the ocean tide signal not recovered by the Cartwright and Ray ocean tide model. This is done in a global analysis where spherical harnomic expansions to degree 18 of the components are estimated simultaneously using 34 cycles of Topex/Poseidon altimeter data. The results show that the annual signal at these wavelengths has a magnitude of 2.5 cm. On the northern hemisphere the annual variability is found to reach its maximum values (8-1 O cm) in October. On the southern hemisphere the phases are shifted six months. Semiannual variability of 2-3 cm is found in the western parts of the equatorial Pacific and has it maximum values in April and in October. The ocean tide residual corrections are small: 2.7 cm (M_2), 1.3 cm (S2), 1.5 cm (K_1), and 0.8 cm (01), all root-mean-square, respectively. However, M2 residuals of 6-8 cm are found. Although the K_1 ocean tides has an aliased period of 173 days, the K_1 and the semiannual variability can be separated in the equatorial regions when altimeter data from both ascending and descending tracks are used.

1, Visiting at Jet Propulsion Laboratory, California Institute of Technology, 4800 Oak Grove Dr., MS 300-323, Pasadena, CA 91109, USA, until May 1, 1994.

Introduction

A recovery of the large scale ocean variability from satellite altimetry has previously been hampered by existing errors in the satellite orbits (e.g. Zlotnicki et al., 1989, Koblinsky et al., 1991, and Jacobs et al., 1992). Especially orbit errors associated with a frequency of one cycle per revolution affect directly an estimation of the large scale seasonal changes between the two hemispheres. Also errors in the geophysical corrections for e.g. wet tropospheric effects have caused errors in the estimation of the global variability. With the launch of Topex/Poseidon August 10, 1992 a satellite mission was initiated that would change this situation.

Analysis of the first few months of Topex/Poseidon altimeter data (Interim Geophysical Data Records) showed that the total error of a single sea surface height measurement is about 9 cm (Fu, 1993). This is about three time smaller than for previous satellite missions. The major improvement has been achieved in the orbit determination. Recent analysis using the data from the Geophysical Data Records (Callahan, 1993) indicate that the accuracy is closer to 5 cm; the orbit error is as small as 3 cm (Fu et al., 1993). Hence, radial orbit errors have become so small that they maybe neglegted. Of growing concern through the past years however, is the accuracy of the tidal models, since ocean tides not removed by the tide models are the largest signals in the altimeter data.

In this study the large scale seasonal ocean variability is analysed. This is done in a global analysis using spherical harmonic functions. The long wavelength ocean tide signals not recovered by the Cartwright and Ray ocean tide model (Cartwright and Ray, 1990, 1991) are recovered simultaneously with the annual cycle, and semiannual cycle, and the mean sea surface. Furthermore, the correlations between the seasonal

variability and the ocean tides are analysed using the available 34 cycles of Topex data starting at September 9, 1992.

The Model

An observation of the height of the sea surface above the reference ellipsoid at a location with latitude ϕ, longitude λ, and time t is described as

$$h(\phi,\lambda,t) = h_0(\phi,\lambda) + \zeta(\phi,\lambda,t) + H^T(\phi,\lambda,t) + n \qquad (1)$$

where $h_0(\phi,\lambda)$ is the mean sea surface, $\zeta(\phi,\lambda,t)$ is the sea surface variability, $H^T(\phi,\lambda,t)$ is the ocean tides, and n is the error of the observation, The use of cross-over or collinear height differences would eliminate the mean sea surface height from the observation equation (e.g. Fu and Chelton, 1985, Milbert et al., 1988, and Tai, 1988). In this study, however, the mean sea surface was included in order to faciliate a study of the possible correlations between this surface and the other height components.

The sea surface variability contains a variety of frequencies. Actually, the spectrum is continous and infinite. Here only the frequencies associated with the annual and the semiannual cycles are considered. The ocean tides are also associated with well defined frequencies determined by the forcing of the moon and the sun (Cartwright, 1993). Then

$$h(\phi,\lambda,t) = h_0(\phi,\lambda) + \sum_{k=1}^{K} \left(U_k(\phi,\lambda)\cos(\omega_k t+\chi_k) + V_k(\phi,\lambda)\sin(\omega_k t+\chi_k) \right) + e \qquad (2)$$

where the ocean variability together with the ocean tides have been expressed in terms of K frequencies, ω_k. For the ocean tides χ_k are the astronomical phases that relate the ocean tides to the phases of the tidal potential; else they maybe set to zero. $U_k(\phi,\lambda)$ and $V_k(\phi,\lambda)$ are surfaces of the cosine and the sine coefficients respectively. Now the error e contain both the observational error n of equation (1) and variability at frequencies different from the K frequencies ω_k. The amplitudes, $A_k(\phi,\lambda)$, and phases, $P_k(\phi,\lambda)$, respectively are easily obtained from the cosine and sine coefficients. Then eq.(2) is

$$h(\phi,\lambda,t) = h_0(\phi,\lambda) + \sum_{k=1}^{K} A_k(\phi,\lambda)\cos\left(\omega_k t + \chi_k - P_k(\phi,\lambda)\right) + n \qquad (3)$$

where $A_k(\phi,\lambda)^2 = U_k(\phi,\lambda)^2 + V_k(\phi,\lambda)^2$ and $P_k(\phi,\lambda) = \arctan\left(V_k(\phi,\lambda)/U_k(\phi,\lambda)\right)$. The coefficients have been estimated as constants over small areas such as boxes (e.g. Zlotnicki et al., 1989, Cartwrigt and Ray, 1990, Woodworth and Thomas, 1990, Jacobs et al., 1992, and Knudsen, 1993c). In this study the surfaces are approximated by spherical harmonic expansions such as in the global analysis of the dynamic sea surface topography carried out by e.g. Engelis and Knudsen (1989), Marsh et al. (1990), Wagner (1986), and Tapley et al. (1988). For $U_k(\phi,\lambda)$ that is

$$U_k(\phi,\lambda) = \sum_{l=1}^{L}\sum_{m=0}^{l}\left(C_{klm}\cos(m\lambda) + S_{klm}\sin(m\lambda)\right)P_{lm}(\sin\phi) \qquad (4)$$

where the harmonic expansion has been truncated at harmonic degree and order L. Similar expressions for the $h_0(\phi,\lambda)$ and $V_k(\phi,\lambda)$ surfaces are used. Spherical harmonic functions have been used in estimations of the M2 ocean tide (Mazzega, 1985) and of

the seasonal cycles (Koblinsky et al., 1991) respectively. The advantage of such parameters is that information is taken into account globally in the estimation of the surfaces and not just the observations located within the limits of small boxes. The disadvantage is that the computational requirements are much larger; even if the series have been truncated at a low degree and the spatial resolution hereby has been reduced.

Since altimeter data from a period just under one year are available it was decided to ignore interannual variations. Only the annual and the semiannual cycles are considered together with the four major tidal constituents: M2, S2, K_1, and O_1.

On the Sampling of the Ocean Tides.

The characteristics of how the ocean tides are sampled by the satellite are important to consider when ocean tides are studied using satellite altimetry. The so-called aliased periods describe how signals of periods of one or one half day show up when they are sampled at longer periods such as 10 days. Following Cartwright (1993), Jacobs et al. (1992), Knudsen (1993a), and Parke et al. (1987) the aliased periods due to the sampling of Topex/Poseidon have been computed for the tidal constituents considered in this analysis (see Table 1). The AP127 values are the changes in phase of the tides that are found at the next overflight of the satellite, which occur 127 revolutions or 9.9 days later.

Table 1. Periods, phase changes after 127 revolutions and associated aliased periods, and phase changes efter 38 revolutions anti associated spatial wavelengths along equator,

Constituent	Period [days]	ΔP_{127}	Aliased Period	ΔP_{38}	λ_e
M2	0.5175	57.5°	62.1	-96.20	-10.6°
S_2	0.5000	-60.70	-58.8	-23.80	-42.80
K_1	0.9973	-20.60	-173.3	-9.0°	-113.40
O_1	1.0758	78.10	45.7	-87.20	-11.7°

The aliased periods of M2 and S2 are both about 60 days and for O_1 it is shorter, The aliased period of K_1, however, is 173 days. Hence, along one set of collinear tracks, residual K_1 ocean tide signals will appear as semiannual variability. They are indistinguishable unless neighboring tracks show very different phases.

The spatial behaviour of the tides as measured by the satellite can be analysed by considering the changes in phase occuring between neighboring parallel tracks. The nearst track to the east occur 38 revolutions (about three days) later. The AP38 values in Table 1 show the phase changes after these three days. A small value such as -9° means that the K_1 ocean tide is in nearly the same phase at neighboring tracks. The spatial wavelengths along the equator in Table 1, λ_e, is obtained using the ΔP_{38} values and the spacing between the neighboring parallel tracks at equator (2.8350). Hence, the small phase lag of the K_1 component corresponds to a long spatial wavelength (1 13.40). Unfortunately, this means that residual K_1 signals and semiannual variability cannot be separated at shorter wavelengths using parallel tracks.

A combination, however, of both ascending and descending tracks will solve the problems described above, if the phases of the tides at crossovers of the ascending and

the descending passes are shifted significantly. On the equator the nearst crossing track to the east arrives about 1.52 days later. Roughly, after 1.5 days the phases of the diurnal constituents (e.g. K_1 and O_1) are shifted by 1800, while the semidiurnal constituents (e.g. M_2 and S2) are in the same phases. Hence, at the equator the diurnal tides can be recovered using both ascending and descending tracks.

Moving away from the equator the distance between the equator crossings of the crossing tracks increases. Therefore the phase differences change according to these equatorial distances in relation to the λ_e and the AP38 values in Table 1 independently on the longitude. E.g. the phases of K_1 at crossing tracks will change by 180^o and . hereby become zero at latitudes where the distances between the equator crossings are 56.70. Here, i.e. at latitudes around 500N and 500S information from combining ascending and descending tracks does not improve the situation with respect to a separation of K_1 and semiannual variability.

Data Selection and Estimation

The mean sea surface, the annual cycle, the semiannual cycle, and the four tidal constituents are taken into account in the modelling of the sea surface (eq. 1). Splitting the time dependent terms into cosine and sine terms, equation (2), this leaves 13 surfaces to be estimated.

An expansion of each of the 13 surfaces into series of spherical harmonic functions, equation 4, results in a large number of coefficients to be estimated. A series complete to harmonic degree and order L consists of $(L+1)(L+2)-1$ coefficients. Due to memory

constraints during the computations it was decided to solve for harmonic coefficients up to harmonic degree and order 18 for all 13 surfaces.

Spherical harmonic degree 18 roughly corresponds to wavelengths about 200 or 2220 km. Therefore an along track sampling of 555 km was choosen for the altimeter data, so that data of different passes are selected at the same locations. 34 passes of Topex GDR altimeter data (Callahan, 1993) covering a period of 340 days from September 9, 1992, were used in this study. In order to avoid aliasing caused by gaps in the data distribution it was decided to **eliminate observations at locations having** fewer than 23 observations present. This primarily eliminated observations close to 660S where no winter observations are available, probably due to sea ice. The selection of observations resulted in 138,865 sea surface height observations located at 4,638 points. Hence, 30 samples on average are available at each selected location. The geographical distribution of the selected observation is shown in Figure 1.

In addition to the standard corrections (altimeter sensor effects, electromagnetic bias, ionosphere, wet troposphere, and dry troposphere) also a 100 % inverse barometer correction was applied (Callahan, 1993). Geophysical corrections for ocean tides, earth tides, and pole tides were applied using the ocean tide model by Cartwright and Ray (1990, 1991). The mean sea surface heights obtained from the Ohio State University (Basic and Rapp, 1992) were subtracted together with an empirically determined systematic difference between the Topex altimetry and the Ohio State Mean Sea Surface. That is

$$\Delta h(\phi,\lambda,t) = h(\phi,\lambda,t) - h_{OSU}(\phi,\lambda) - 0.243 \cos\phi \sin\lambda - 0.400 \quad [m] \qquad (5)$$

where $h_{OSU}(\phi,\lambda)$ is the Ohio State Mean Sea Surface. The systematic difference has been associated with a shift of the center of the reference frame along the Y axis by 24 cm and a bias of 40 cm (Rapp, privat communication, November 1993). The shift along the Y axis is probably related to a dislocation of the reference frame of the Geosat orbits. The bias also contain the altimeter bias which is about 18-20 cm. The surface $h_0(\phi,\lambda)$ of equation (1) hereby becomes a correction to the Ohio State Mean Sea Surface.

Subtracting the Ohio State Mean Sea Surface and the systematic difference serves two purposes: The first purpose is to remove short wavelength geoid signals that otherwise may cause aliasing errors, The second purpose is to remove known long wavelength parts of the sea surface heights. This is actually done in order to reduce effects known to exist when spherical harmonic functions are used on the oceans only. The problem occurs because the spherical harmonic functions do not form an orthogonal set of base function over the oceans as they do over the whole surface of the sphere. Then serious correlations between the coefficients exist, e.g. all coefficients may become affected by a bias in the data (Engelis and Knudsen, 1989, Denker and Rapp, 1990, and Hwang, 1991).

The mean value of the 138,865 selected observations after reduction became zero. The standard deviation is 0.190 m.

The estimation of the unknown coefficients was carried out using standard least squares techniques taking into account the variances of both the signal and the noise. If equation (1) is expressed as $y = Ax$ where y and x are vectors of the observations and the unknown coefficients respectively, and A is a matrix. Then the unknowns can be estimated from the observations by

$$x = \left(A^T C^{-1} A + D^{-1}\right)^{-1} A^T C^{-1} y \qquad (6)$$

where C and D are covariance matrices associated with the coefficients and the noise respectively. Both covariances matrices are assumed to be diagonal. Through the D matrix the observations are weighted using $1/\cos\phi$ in order to compensate for the increased data density at high and low latitudes. As *a-priori* standard deviations of the coefficients, a degree variance model, σ_l, was applied. Empirical degree variances obtained from analysis of the Levitus sea surface topography (e.g. Figure 6.6 in Hwang, 1991) show thatthe degree variances decreases with increasing harmonic degree. Here $\sigma_l = 1/l^2$ [m2] was used for all the surfaces.

Results

The solution was first evaluated by comparing the observations with estimates obtained using the estimated coefficients. These results are summarized in Table 2.

Table 2. Root-Mean-Square values of observations and quantities estimated in the observation points. Also the numerically largest values are shown.

Quantity	RMS [cm]	Maximum [cm]
Observations	19.0	293.2
Estimates	8.7	61,5
Reduced observations	16.1	250.0
Mean sea surface	7.5	47.5
Annual cycle	2.5	10.4
Semiannual -	1.0	4.9
M2	2.7	7.6
S_2	1.3	4.4
K_1	1.5	4.1
O_1	0.8	2.8

The root-mean-square (RMS) value of the observations has been brought down from 19.0 cm to 16.1 cm. A considerable part of these numbers is associated with geoid undulations at wavelengths shorter than 2220 km. However, the variance has been reduced by (10.1 cm)2 and the largest estimate is 61.5 cm, so the solution actually accounts for a considerable part of the observed values. (The variance reduction can be larger than the variance of the estimates if the quantities are not fully uncorrelated.)

The individual quantities are small in average (-l-able 2). The residual ocean tides (i.e. those tides not removed by the Cartwright and Ray model) have about the same' magnitudes as the seasonal variability. The M2 itself has the same magnitude as the annual cycle and the S2 and the K_1 are larger than the semiannual cycle. The O_1 appears to be insignificant.

The Mean Sea Surface

The most significant quantity is the mean sea surface height differences relative to the Ohio State Mean Sea Surface. The RMS value is 7.5 cm and the largest difference is 47.5 cm. The systematic differences corresponding to the shift along the Y axis and the bias are not included in these values. A contour map is shown in Figure 2. This map shows that values exceeding 10 cm are found in the western equatorial region of the Pacific and the Atlantic oceans, in the central part of the Indian Ocean, and in the Mediterranean Sea. At high latitudes on the northern and the sounthern hemispheres negative values are found. The normalized harmonic coefficients C_{20} is -6.1 cm, which corresponds to a difference of 6.8 cm and -12.3 cm at the equator and poles respectively.

The differences may be due to inaccuracies in the Ohio State Mean Sea Surface. The original wet tropospheric corrections that were used on Geosat were based only on the surface water vapor (FNOC) and integrated assuming a height profile that is not valid near the equator. This results in systematic errors of 10-15 cm at the equator (Liu et al., 1992, Zlotnicki, 1994). The Topex/ Poseidon correction is based on direct measurements of the integrated water vapor profile.

In the equatorial Pacific Ocean the largest differences are found in the western parts of the ocean. Here the warmest water is found from which the highest rate of evaporation takes place. A similar situation is found in the Indian Ocean. However, it is important to consider that this mean sea surface represents an average over the first 34 cycles of the Topex/Poseidon mission. The Ohio State Mean Sea Surface is calculated from observations covering a different epoch of time.

The Seasonal Variability

The magnitudes of the annual and the semiannual cycles to harmonic degree and order 18 are 2.5 cm and 1.0 cm (RMS) respectively (-[able 2). The amplitudes and the phases were computed from the cosine and the sine coefficients according to equation (3). Both amplitudes and phases for the seasonal cycles are shown in Figure 3-4.

The amplitudes of the annual cycle are largest on the northern hemisphere between latitudes 25-500N (Figure 3). Here amplitudes larger than 8 cm are found in the Kuroshio and in the Gulf Stream regions. The phase map (also Figure 3) show that these variations of the Kuroshio and the Gulf Stream adopt their maxima in the first half and in the second half of October respectively. l-his agree with the results by Zlotnicki (1991) and by Jacobs et al. (1992). In the Mediterranean Sea an annual variation having a similar phase (late October) is found. It has an amplitude of 5-6 cm in the western and the central parts of the sea.

On the southern hemisphere between latitudes 25-50°S amplitudes of 2-4 cm are found centered at the Agulhas, the Brazil-Malvinas, and the east Australian currents. Those variations reach their highs in March, so also on this hemisphere the maximum values occur around the fall equinox. Closer to the equator, i.e. latitudes of 10-200, on both hemispheres the annual variability occur one or two months earlier.

In the equatorial regions annual variations of 2-4 cm are found in the Pacific Ocean. In the central parts maximum is reached in December. The magnitude of the annual variability found by Jacobs et al. (1992) in the equatorial regions is much larger, but due

to inaccurate water vapor correction this variability may rather reflect an annual change in the atmosphere (also Zlotnicki et al., 1989, Zlotnicki, 1993). Furthermore, the changes in the equatorial currents and counter currents may occur on spatial scales too small to be recovered in this analysis.

The annual variability show a significant latitude dependent pattern. However, in the north-western part of the Indian Ocean a 5 cm variation is found that has its maximum around April, so it does not follow the normal pattern. This may be due to the variations of the Monsoon winds.

Semiannual variability is found in the western parts of the equatorial Pacific (Figure 4). It has amplitudes of about 2-3 cm and maximum values occur in April and in October. Smaller signals are found at equator off the west coasts of the American and the African continents. The strongest semiannual signals are found in the Indian Ocean. Here 3-4 cm amplitudes are found off the African coast and in the north-eastern parts of the Indian Ocean. The phases change from late March (and late September) in the western part of the ocean to 2 months later (late May and November) in the north-eastern parts of the Indian Ocean.

Off the equatorial regions semiannual variability of a few centimetres is found in the same regions as where the annual variability is seen (compare Figure 3-4). The variations at the Brazil-Malvinas and the east Australian currents are in opposite phases and smaller that the annual variation. Hence, semiannual variability in these regions are believed to be due to a not purely sinusoidal annual cycle.

Residual Ocean Tides

l-he amplitudes of the residual M2, S_2, and K_1 ocean tides are shown in Figure 5-7 respectively (O_1 is not shown). M2 amplitudes larger than 5 cm are found in the east central Pacific, the central south Pacific, the Indian, and the east South Atlantic Oceans (Figure 5). The phases (not shown) of these four discrepancies are about 1200,-1500, -900, and -100 respectively. Hence, these phases are about minus the longitudes of the locations of the residual signals. This maybe a coincidence, but it indicates that there may be a problem in the determination of the tidal arguments,

S2 larger than 3 cm is mainly found in the equatorial regions of the eastern Pacific, the central Indian, and to some extent the Atlantic oceans (Figure 6). In contrast K_1 residuals larger than 3 cm in amplitude are found off the equator south-west of the coasts of Africa, Australia, and South America. Also in the north east Pacific K_1 residuals larger than 3 cm are found (Figure 7).

Fortunately, the results from the previous analysis of the ocean tide aliases show that the large M2 residuals and the S2 residuals should not affect an estimation of the seasonal variability, since both constituents have aliased period about 60 days. Unfortunately, the K_1 residuals may have done so off the equatorial regions.

Error Analysis

in order to analyse the error correlations between the mean sea surface, the seasonal variability, and the residual ocean tides, error correlations between the amplitudes of each of the quantities were computed. Due to computational constraints this was only carried out for quantities located in the Pacific between $\pm 45^{o}$ latitude. The correlations

are summarized in Table 3.

Table 3. Correlation coefficient range between quantities computed in the Pacific Ocean between ±45° latitude. Units are %.

Quantity	Mean	Annual	Semi-	M_2	S_2	K_1	O_1
Mean surface	-	-11>-6	-3>-1	-4>2	-5>5	-2>1	-1>2
Annual cycle	-11>-3	-	-2>2	-3>3	-9>8	-3>3	-3>2
Semiannual -	-3>-1	-2>2	-	-2>2	-4>2	-26>27	-1>1
M2	-4>2	-3>3	-2>2	-	-9>11	-1>2	-3>3
S_2	-5>5	-9>8	-4>2	-9>11	-	-3>2	-4>3
K_1	-2>1	-3>3	-26>27	-1>2	-3>2	-	-3>1
O_1	-1>2	-3>2	-1>1	----3>3	-4>3	-3>1	-

Most of the error correlations listed in Table 3 are small. Actually, they are so small that most of the quantities are uncorrelated. An important result is that the estimated mean sea surface, the annual cycle, and the semiannual cycle are not correlated with the M2 ocean tides. The O_1 tide correlations do not cause alarm either. The mean sea surface and the annual cycle are not correlated with the K_1 ocean tides, but as expected the semiannual cycle and the K_1 tides are considerably correlated.

The mean sea surface and the annual cycle appear to be slightly correlated. This is probably caused by the fact that data from a period less than one year is used. This, however, does not cause any correlations between these quantities and the semiannual cycle. Unexpected is the correlations between the annual cycle and the S2 ocean tides, since the aliased period of S2 is -58.8 days, substantially shorter than a year. Although being small these correlations will be further analysed below.

A global map of the errors of the mean sea surface is shown in Figure 8. These errors have been obtained using an observational error of 16 cm, which corresponds to how well the observations are fitted by the model (Table **2).** The errors are small over the oceans and higher on land. Over the oceans the accuracy of the mean sea surface heights are **0.5 cm.** The errors of the other surfaces, i.e. the cosine and the sine coefficients, turned out to be about 15 % higher. Therefore, the errors of the amplitudes are about 0.8 cm. The correlations between the mean sea surface and the annual cycle are shown in Figure 9. The correlations are about -9 %, but in the southern ocean where the coverage may be poorer (23 samples out of 34) -12 % is found. Outside the region covered by data the errors increase and the correlations vanish.

The correlations between the annual cycle and the S2 tidal component are shown in Figure 10. They show a very characteristic pattern, where they adopt their minimum and maximum values on equator following a two cycle variation around the earth. Hence, it appears that these correlations depend on a semidiurnal modulation of a surface containing even zonal harmonic functions only. A closer evaluation of the correlation matrix reveals correlations of 3-4 % between the sectorial harmonic functions of degree one (i.e. l=m=1) of both quantities, and between the sectorial harmonic functions of degrees 3 and 5 of each surface respectively and vise versa. In general correlations between sectorial spherical harmonics (i.e. l=m) of harmonic degrees separated by two are seen.

Figure 11 shows the correlations between the semiannual cycle and K_1. In contrast to the previous correlations these correlations are zero on equator as expected for a diurnal tidal constituent. **Moving away from equator the correlations increase and reach** 55 % in the southern Pacific. Also, as expected negative correlations are found in the northern Pacific. However, on the southern hemisphere the largest negative correlations

are **found in the Indian Ocean in a distance** from the maximum correlations of 1800 in longtude. Hence, a diurnal modulation of odd zonal harmonic functions appear to determine the pattern of these correlations. A closer evaluation of the correlation matrix reveals a correlations of 18 % between the harmonic functions of degree two and order one (i.e. l=2, m=l) of both quantities. Additional correlation of 11-14 % are found between the first order harmonic functions of degrees 1 and 4 of each surface respectively, and between first order harmonic functions of degrees 2 and 4 of each surface respectively and vise versa, Furthermore, correlations between spherical harmonics separated by one in both harmonic degree and order are found.

An obvious analytical explanation for the pattern of the correlations does not exist, but the actual distribution of the observations, i.e. the lack of data over land, is believed to be the main factor. The important result is that the major correlations existing between the semiannual cycle and K_1 also in practice are found outside the equatorial region at high and low latitudes hampering studies of the semiannual cycles of the Antarctic Circumpolar and the Alaska currents only.

Discussion

This analysis of the seasonal variability has shown that the large scale annual changes in sea level successfully can be recovered using Topex/Poseidon altimeter data. At latitudes of 20-500 the annual cycle clearly shows rising sea level through the summer season and falling sea level through the winter season. The largest amplitudes are found on the northern hemisphere. Hence, the results agree well with the results of Jacobs et al. (1992). In the equatorial regions, however, results from Topex/Poseidon are not affected by inaccuracies of the wet troposphere corrections.

The mean sea surface differ from the Ohio State Mean Sea Surface in the C_{20} coefficient by -6.1 cm (normalized). Again the inaccurate wet troposphere corrections of Geosat are believed to cause most of these differences. The difference is important in studies of the permanent circulation and the determination of the shape of the static sea surface topography. A recovery of the short wavelength signals may be recovered accurately on regional scales (Knudsen, 1991, 1993b). An improved reference surface will also be **extremely valuable in the removal of systematic errors from altimetry of other satellites such as ERS-1 (Knudsen et al., 1992).**

The ocean tide residuals recovered in this analysis agre very well with results by Fu et al. (privat communication, October 1993). A detailed analysis of how the ocean tides may affect the estimation of the seasonal variability showed that K_1 ocean tides can be separated from semiannual variability in the equatorial regions even though its aliased periode is close to half a year. The O_1 residuals are so small that they be disregarded in future analysis.

During this analysis it was assumed that both orbit errors and errors in the wet tropospheric correction are sufficiently small to be left out. Also the inverse barometer has been applied 100 %. Future analysis of Topex/Poseidon altimetry will show wheater this was reasonable. A valuable control of the orbit accuracy can be performed using the upcomming GPS orbits, but considerable improvements of the seasonal variability requires observations from more than one year.

Acknowledgement. **This analysis primarily supported by Kort- og Matrikel-styrelsen (the National Survey and Cadastre - Denmark) was carried out at the Jet Propulsion Laboratory, California Institute of Technology, under contract with the National Aeronautics and Space Administration, with partial support**

from the Topex/Poseidon Project. Travel fends have been provided by the Danish Research Foundation and Kort- og Matrikelstyrelsen. Software by T.L. Engelis was used. Thanks to Victor Zlotnicki for inspirering discussion.

References.

Basic, T., and R.H. Rapp: Oceanwide Prediction of Gravity Anomalies and Sea Surface Heights Using Geos-3, Seasat, and Geosat Altimeter Data and ETOPO5U Bathymetry Data. Report. no. 416, Dept. of Geodetic Science and Surveying, The Ohio State University, Columbus, Ohio, 1992.

Callahan, P: Topex/Poseidon Project GDR Users Handbook, JPL D-8944, rev A, 84 pp. Available from Distributed Active Archive Center, Jet Propulsion Lab. 300-319,4800 Oak Grove Dr., Pasadena, CA 91109, USA, 1993.

Cartwright, D. E.: Theory of Ocean Tides with Application to Altimetry. In: R. Rummel and F. Sanso (Eds.): Satellite Altimetry in Geodesy and oceanography, Lecture Notes in Earth Sciences, 50, Springer-Verlag, 100-141, 1993.

Cartwright, D. E., and R.D. Ray: Oceanic Tides from Geosat Altimetry. J. Geophys. Res. Vol. 95, N. C3, 3069-3090,1990.

Cartwright, D.E. and R.D. Ray: Energetic of Global Ocean Tides from Geosat Altimetry. J. Geophys. Res., Vol. 96, N. C9, 16897-16912,1991.

Denker, D., and R.H. Rapp: Geodetic and Oceanographic Results from the Analysis of One Year of Geosat Data. J. Geophys. Res., Vol. 95, N. C8, 13151-13168, 1990.

Engelis, T., and P. Knudsen: Orbit Improvement and Determination of the Oceanic Geoid and Topography from 17 Days of Seasat Data. Manuscript Geodactica, Vol. 14, N. 3,193-201, 1989.

Fu, L.-L. (Ed.): TOPEX/Poseidon Verification Workshop, A Summary Report. JPL D-1 0815, May 24, 1993.

Fu, L.-L., and D.B. Chelton: Observing large-scale temporal variability of ocean currents by satellite altimetry: With application to the Antartic circumpolar current. J. Geophys. Res., Vol. 90, No. C3, 4721-4739,1985.

Fu, L.-L., B, Haines, and G. Pihos: Along-track Frequency Spectrum: Characteristics of the Orbit Errors or Other Variabilities? Topex/Poseidon Research New, Issue 1,18-19, September 1993.

Hwang, C.: Orthogonal Functions Over the Oceans and Applications to the Determination of Orbit Error, Geoid and Sea Surface Topography from Satellite Altimetry. Report no. 414, Dept. of Geodetic Science and Surveying, The Ohio State University, Columbus, 1991.

Jacobs, G.A., G.H. Born, M.E. Parke, and P.C. Allen: The Global Structure of the Annual and the Semiannual Sea Surface Height Variability From Geosat Altimeter Data, J. Geophys. Res., Vol. 97, N. Cl 1, 17813-17828,1992.

Knudsen, P.: Simultaneous Estimation of the Gravity Field and Sea Surface Topography From Satellite Altimeter Data by Least Squares Collocation. Geophysical Journal International, Vol. 104, No. 2,307-317, 1991.

Knudsen, P.: Altimetry for Geodesy and Oceanography. In: Kakkuri, J. (Ed): Geodesy and Geophysics. Lecture notes for the NKG Autumn School 1992, Publications of the Finnish Geodetic Institute, No. 115, Helsinki, 1993a.

Knudsen, P.: Integration of Altimetry and Gravimetry by Optimal Estimation Techniques. In: R. Rummel and F. Sans¢ (Eds.): Satellite Altimetry in Geodesy and Oceanography, Lecture Notes in Earth Sciences, 50, Springer-Verlag, 453-466,1993.

Knudsen, P.: Separation of Residual Ocean Tide Signals in a Collinear Analysis of Geosat Altimetry. Bulletin Geodesique, in press, 1993s.

Knudsen, P., O. Baltazar Anderson, and C.C. Tscherning: Altimetric Gravity Anomalies in the Norwegian-Greenland Sea - Preliminary Results from the ERS-1 35 days Repeat Mission. Geophys. Res. Lett., Vol. 19, No. 17,1992.

Koblinsky, C.J., R.S. Nerem, S.M. Klosko, and R.G. Williamson: Global Scale Variations in Sea Surface Topography Determined from Satellite Altimetry. Presented IUGG XX General Assembly, Symposium U 13, Vienna, 11-24 August, 1991.

Liu, W.T., W. Tang, and F. Wentz: Precipitable Water and Surface Humidity over Global Oceans from Special Sensor Microwave Imager and European Center for Medium Range Weather Forecasts, J. Geophys. Res., 97 (C2), 2251-2284,1992.

Marsh, J.G., C.J. Koblinsky, F.J. Lerch, S.M. Klosko, T.V. Martin, J.W. Robbins, R.G. Williamson, and G.B. Patel: Dymanic Sea Surface Topography, Gravity, and Improved Orbit Accuracies from the Direct Evaluation of Seasat Altimeter Data. J. Geophys. Res., Vol. 95, N. C8, 13129-13150,1990.

Mazzega, P.: M2 Model of the Global Ocean Tide Derived from SEASAT Altimetry. Marine Geodesy, Vol. 9, No. 3,335-383,1985.

Milbert, D., B. Douglas, R. Cheney, L. Miller, and R. Agreen: Calculation of Sea Level Time Series from Noncollinear GEOSAT Altimeter Data. Marine Geodesy, Vol. 12,287-302,1988.

Parke, M. E., R.H. Stewart, D.L. Farless and D.E. Cartwright: On the choice of orbits for an altimetric satellite to study ocean circulation and tides. J. Geophys. Res., Vol. 92. 11693-11707, 1987.

Tai, C.-K.: On Generating Altimetric Sea Level Time Series from Crossover Differences. Marine Geodesy, Vet. 12,303-313,1988.

Tapley, B. D., R.S. Nerem, C.K. Shum, J.C. Ries, and D.N. Yuan: Circulation from a Joint Gravity Field Solution Determination of the General Ocean. Gephys. Res. Lett., Vol. 15, No. 10, 1109-1112, 1988.

Wagnor, C. A.: Accuracy Estimates of Geoid and Ocean Topography Recovered Jointly From Satellite Alitmetry. J, Geoph. Res., Vol. 91, No. B1, 453-461, 1986.

Woodworth, P. L., and J.P. Thomas: Determination of the Major Semidiurnal Tides of the Northwest European Continental Shelf From Geosat Altimetry. J. Geophys. Res., Vol. 95, No. C3, 3061-3068, 1990.

Zlotnicki, V.: Sea Level Differences across the Gulf Stream and Kuroshio extension. J. Physical Oceanog., 21 (4), 599-609,1991.

Zlotnicki, V.: Quantifying Time-Varying Oceanographic Signals with Altimetry. In: R. Rummel and F. Sanso (Eds.): Satellite Altimetry in Geodesy and Oceanography, Lecture Notes in Earth Sciences, 50, Springer-Verlag, 143-188,1993.

Zlotnicki, V. The Geoid from Satellite Altimetry. In: P. Vanicek and N.T. Christou (eds.): The Geoid and its Geophysical Interpretations, CRC Press, ISBN O-8493-4227-9, 95-110, 1994.

Zlotnicki, V., L.-L. Fu, and W. Patzert: Seasonal Variability in Global Sea Level Observed With Geosat Altimetry. J. Geophys. Res., Vol.94, N. C12, 17959-17969, 1989.

Figure 1: Locations of selected altimeter data.

Figure 2: Mean Sea Surface relative to the Ohio State Mean Sea Surface to harmonic degree and order 18, Contour interval is 5 cm.

Figure 3: Annual cycle to harmonic degree and order 18. Amplitudes (upper figure) and phases (lower) relative to January 1, i.e. 41800 is July 1.

Figure 4: Semiannual cycle to harmonic degree and order 18, Amplitudes (upper figure) and phases (lower) relative to January 1, i.e. 1800 is April 1.

Figure 5: M2 ocean tides relative to the Cartwright and Ray **model to harmonic** degree and order 18. Contour interval is 1 cm.

Figure 6: S2 ocean tides relative to the Cartwright and Ray **model to harmonic degree and order 18.** Contour interval is 1 cm.

Figure **7: K_1 ocean tides relative to the Cartwright and Ray** model to harmonic degree and order 18. Contour interval is 1 cm.

Figure 8: Error estimates of the mean sea surface heights to harmonic degree and order 18. Contour interval is 0.2 cm.

Figure 9: Error correlations between the mean sea surface and the annual cycle. Contour interval is 29'..

Figure 10: Error correlations between the annual cycle and the S2 ocean tides, Contour interval is 2 %.

Figure 11: Error correlations between the semiannual cycle and the K_1 ocean tides. Contour interval is 5 $4..

Figure 1:

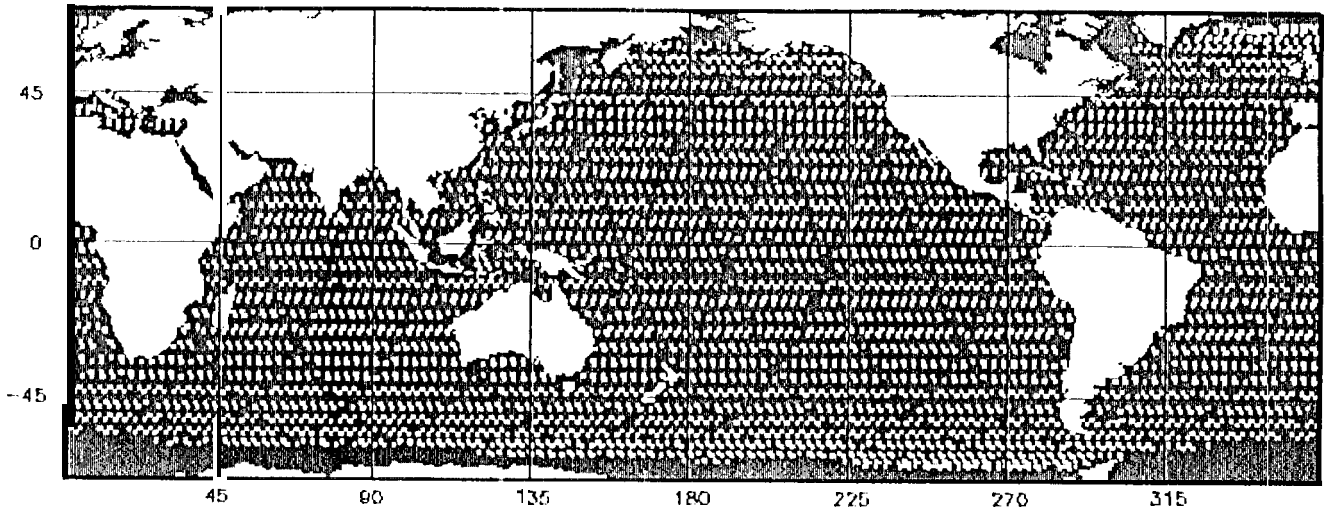

Figure 2: Mean Sea Surface relative to OSU MSS. CI, = 5 cm

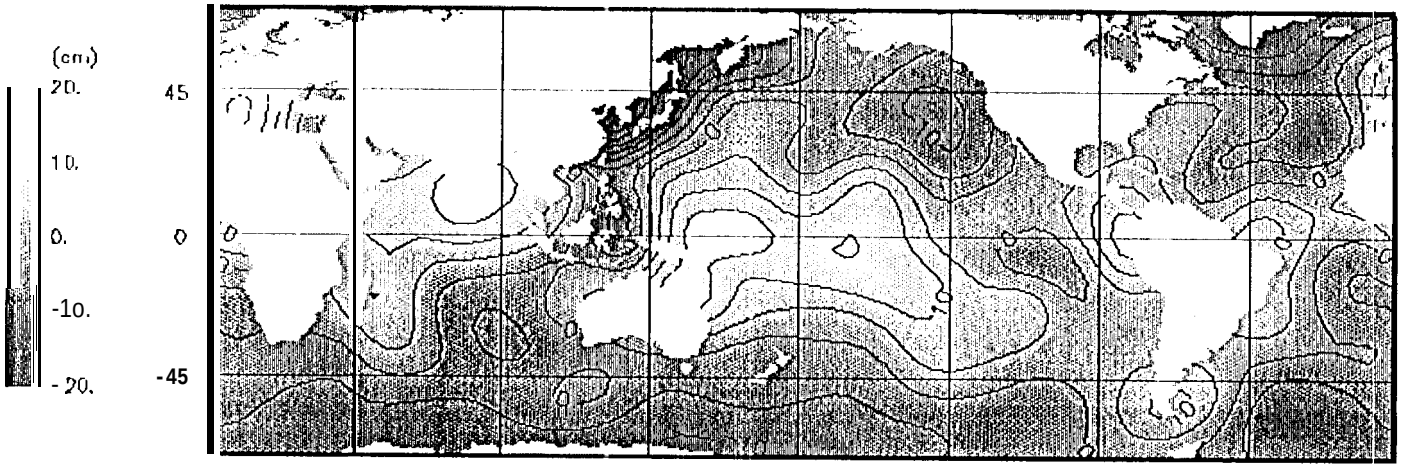

Amplitudes (upper) and Phases (lower) of Annual cycle

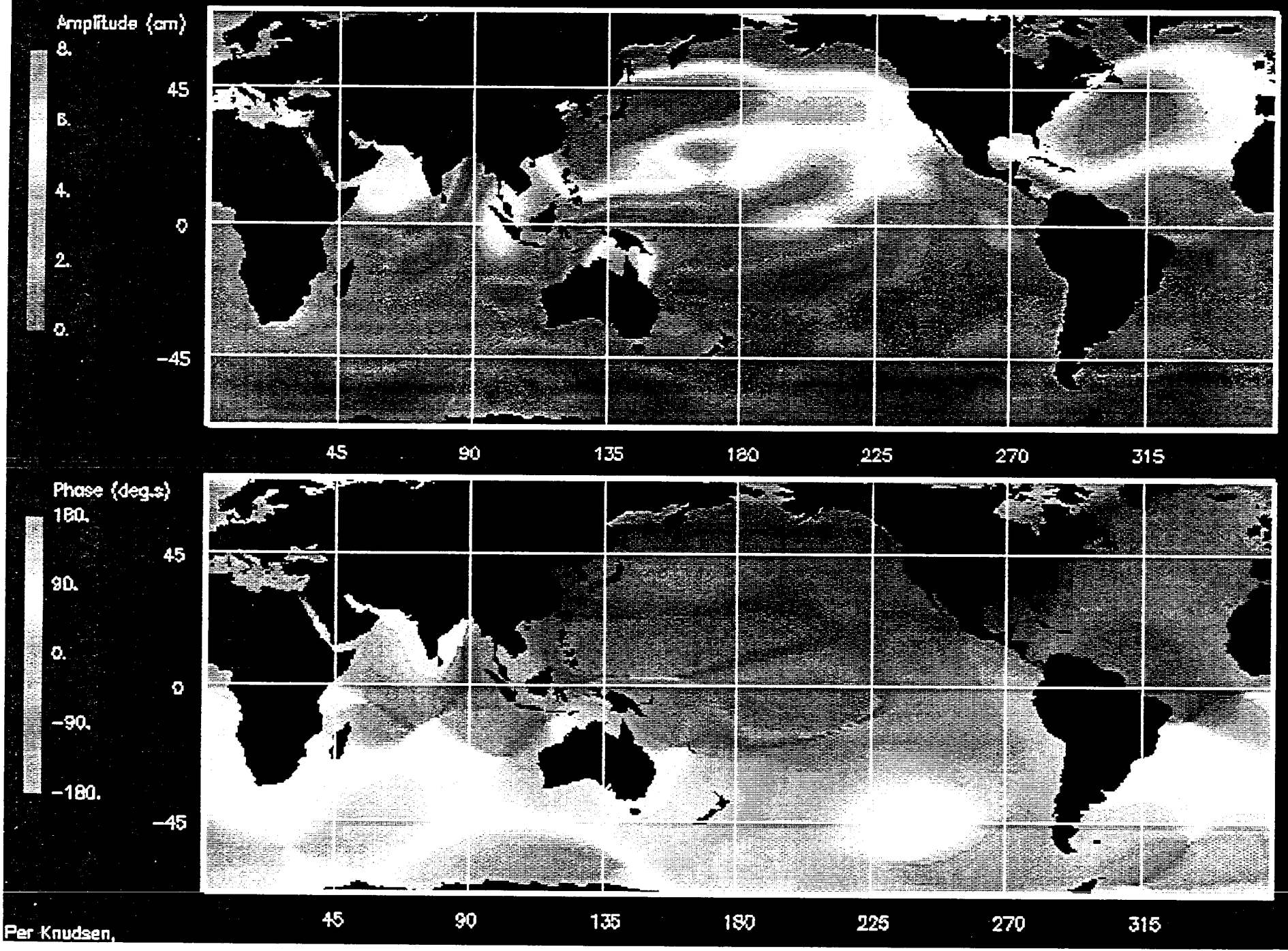

Per Knudsen,

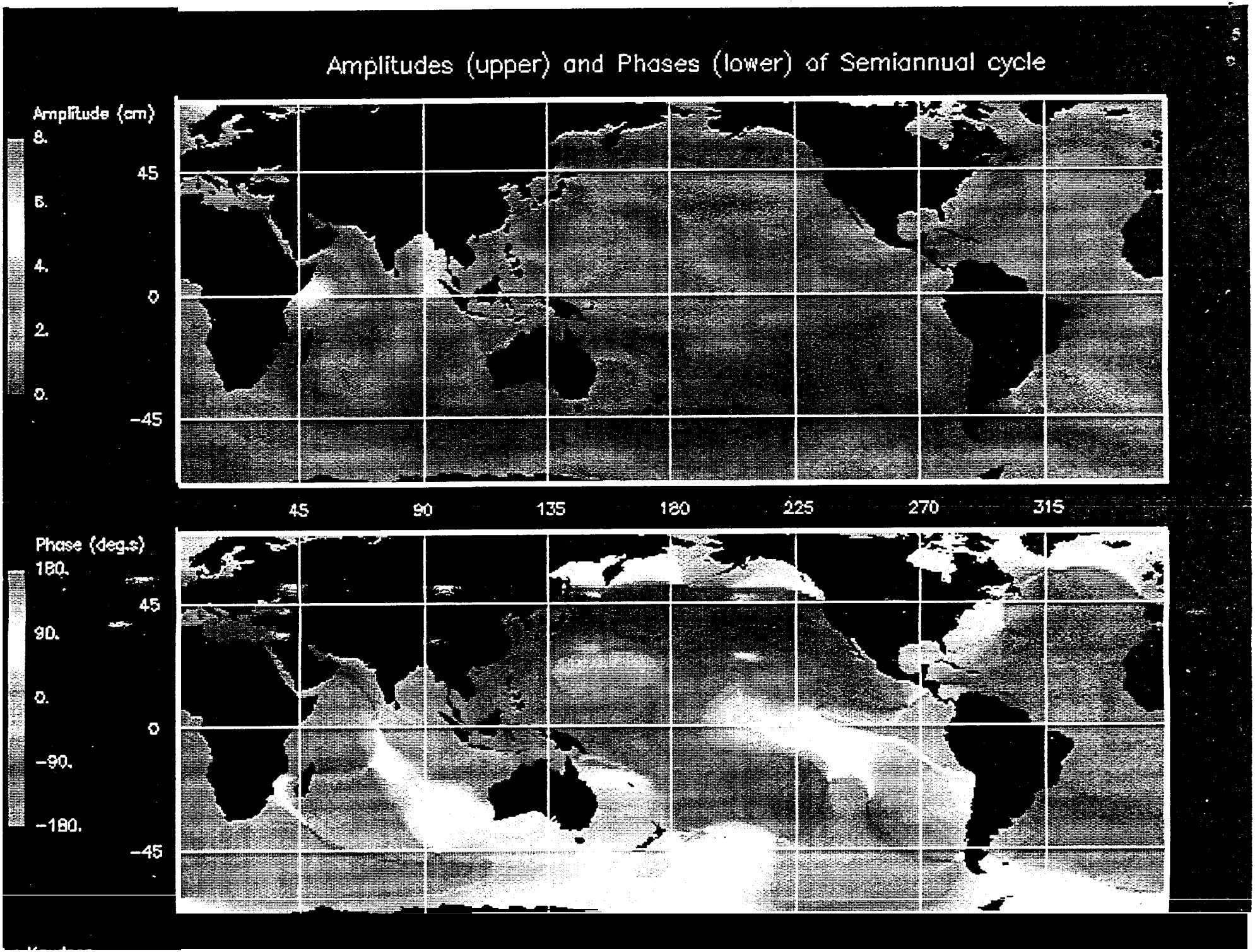
Amplitudes (upper) and Phases (lower) of Semiannual cycle
Amplitude (cm)
8.
6.
4.
2.
0.
45
0
-45
45
90
135
180
225
270
315
Phase (deg.s)
180.
90.
0.
-90.
-180.
45
0
-45

Figure 5:

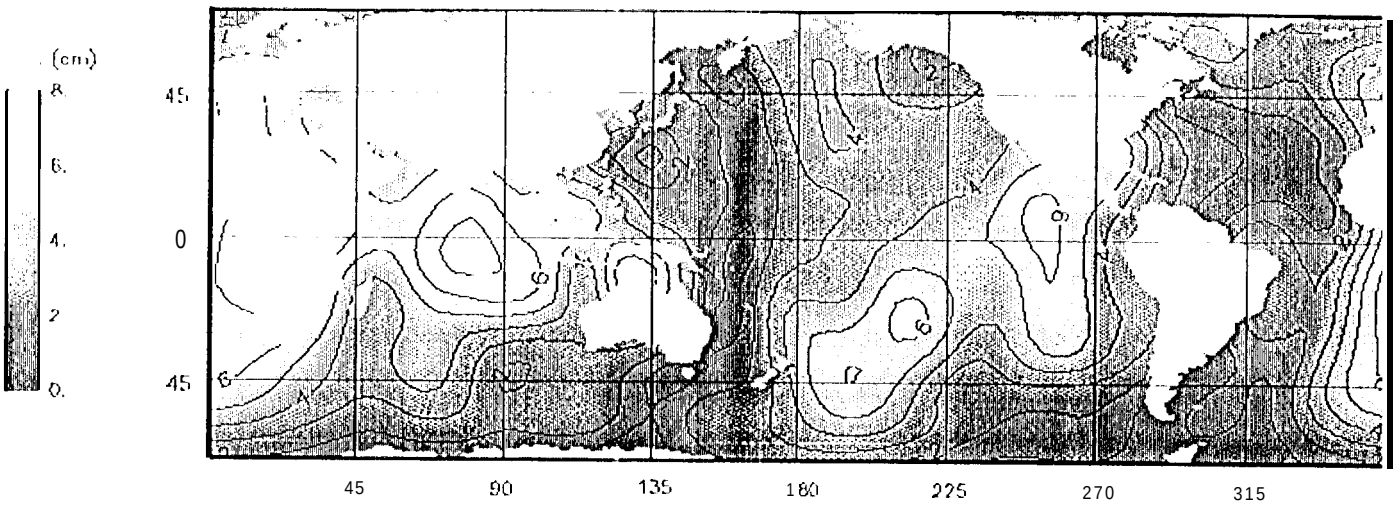

Figure 6:

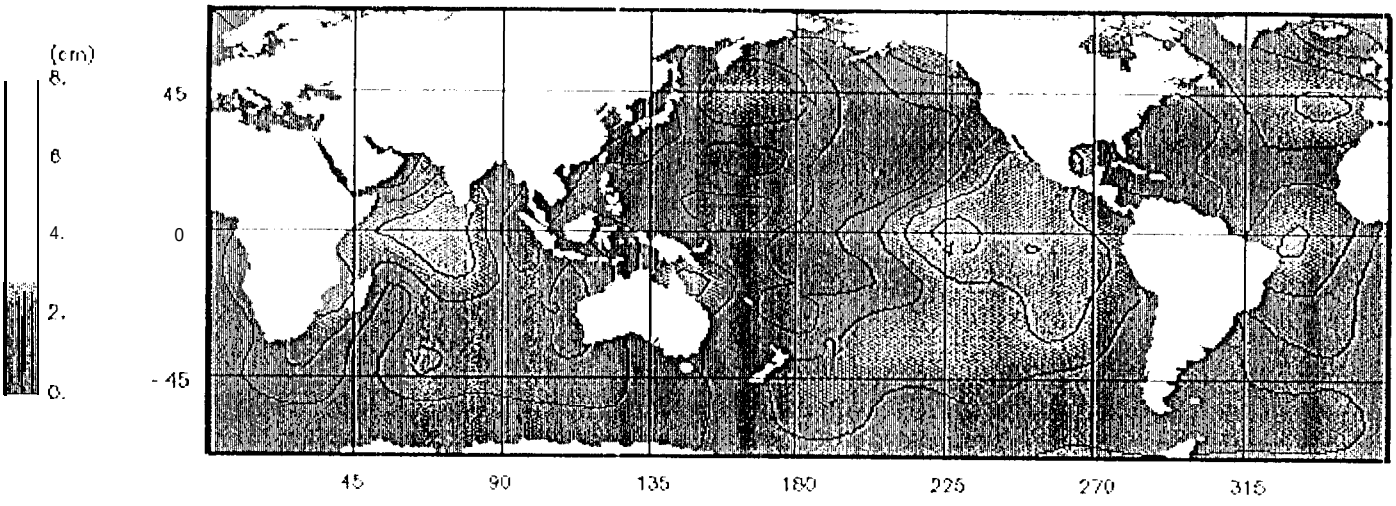

Figure 7:

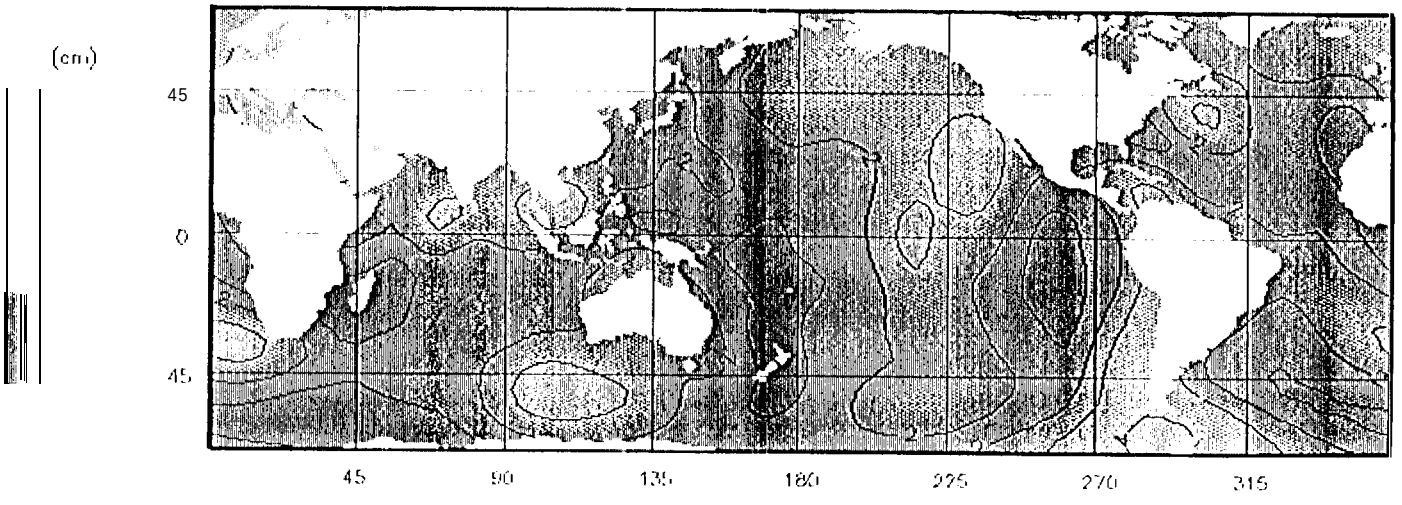

Figure 8: t rrors of **Mean** Sea **Surface** Heights. **Cl. (1. ?** cm

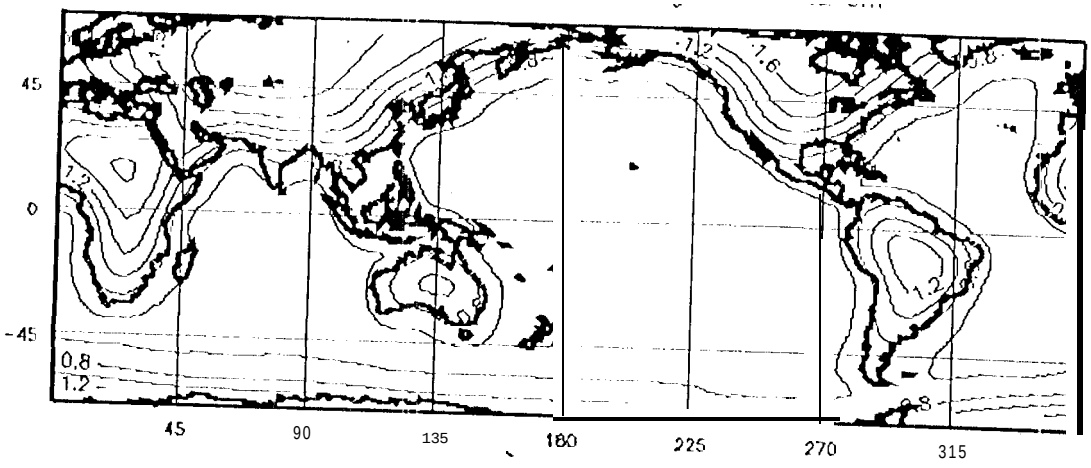

Figure 9: Correlations between **Mean** S urface **and Annual** Cycle. **Cl, 2 %**

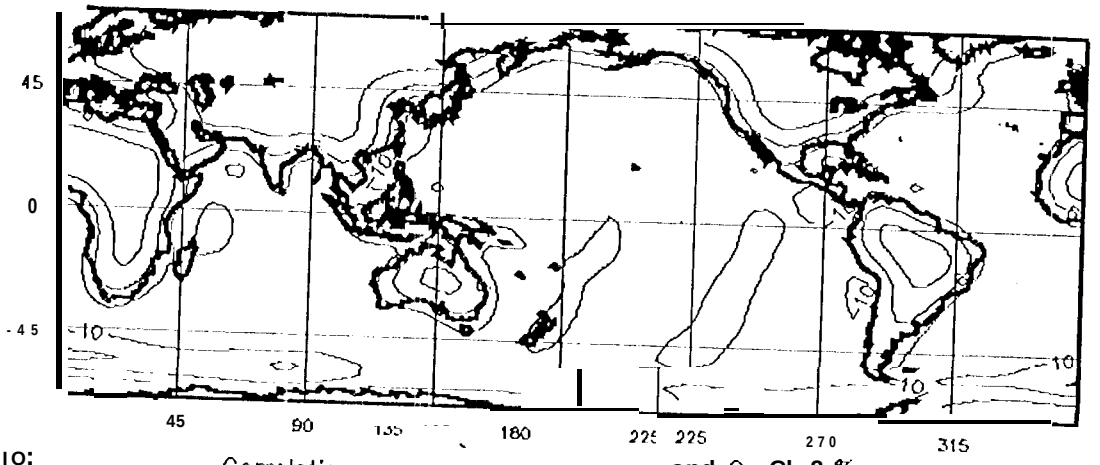

Figure 10: Correlations ween Annual Cycle and **ond** S_2. **Cl, 2 %**

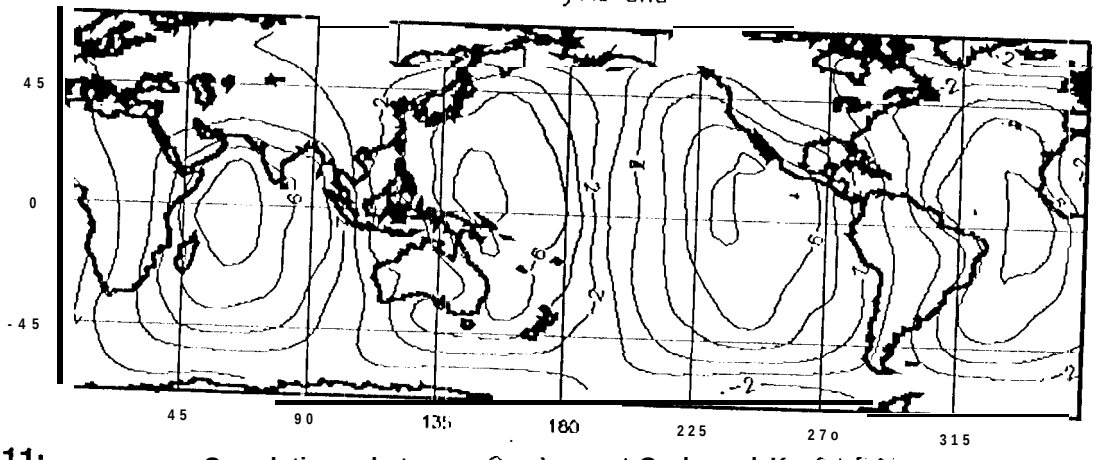

Figure 11: **Correlations between** Semiannual **Cycle and** K_1. C.I. 5 %